# Dirac phonons in two-dimensional materials

Jialin Gong,[1,*] Jianhua Wang,[1,*] Hongkuan Yuan,[1] Zeying Zhang,[2,†] Wenhong Wang,[3] and Xiaotian Wang[1,4,‡]
[1]*School of Physical Science and Technology, Southwest University, Chongqing 400715, China*
[2]*College of Mathematics and Physics, Beijing University of Chemical Technology, Beijing 100029, China*
[3]*Tiangong University, Tianjin 300387, China*
[4]*Institute for Superconducting and Electronic Materials (ISEM), University of Wollongong, Wollongong 2500, Australia*

(Received 12 November 2022; revised 1 December 2022; accepted 20 December 2022; published 28 December 2022)

Phonons are an ideal platform for realizing stable spinless two-dimensional (2D) Dirac points because they have a bosonic nature and hard-to-break time-reversal symmetry. It should be noted that the twofold degenerate nodal points in the phonon dispersions of almost all reported 2D materials are misclassified as "Dirac points" owing to a historical issue. The correct name for these twofold degenerate nodal points should be "Weyl" because 2D phononic systems are essentially spinless and because each twofold degenerate point is described by a Weyl model in two dimensions. To date, reports of fourfold degenerate Dirac point phonons in 2D materials are lacking. In this paper, we searched through all 80 layer groups (LGs) and discovered that Dirac phonons can be realized in 7 of the 80 LGs. Moreover, the Dirac points in the phonon dispersions of 2D materials can be divided into essential and accidental degenerate points, which appear at high-symmetry points and on high-symmetry lines, respectively. Guided by symmetry analysis, we identified the presence of Dirac phonons in several 2D material candidates with six LGs. This work offers a method for identifying Dirac phonons in 2D and proposes 2D material candidates for realizing Dirac phonons.

DOI: 10.1103/PhysRevB.106.214317

## I. INTRODUCTION

The discovery of topological quantum states [1–4] is one of the most promising advancements in condensed matter physics. Currently, the study of topological quantum states is no longer limited to only electron-related systems [5–20] but has been widely extended to include bosonic systems [21–30]. Among the different types of bosonic systems, phonons [31–39], which are induced by atomic vibrations at THz frequency, are a perfect platform for realizing topological quantum states because of their unique advantages and possible applications. Notably, unlike that of electronic bands, the entire frequency range of phonon bands is relevant for experimental detection because phonons are not constrained by the Pauli exclusion principle and Fermi surface. Additionally, topological phonons [31,32,40] play critical roles in thermal transports, electron-phonon coupling, or multiphonon processes.

In the past 5 years, various types of symmetry-enforced topological phonons [40–62], including conventional and unconventional Weyl point phonons, triple point phonons, Dirac point phonons, nodal line phonons, and nodal surface phonons, have been discovered in three-dimensional (3D) realistic materials. Some of them have also been verified through experiments. Two-dimensional (2D) materials have a lower symmetry than 3D materials. Therefore, 2D materials with less symmetrical constraints may more intuitively display the clean characteristics of topological phonons. Unfortunately, topological phonons have only been explored in only a few 2D materials [63–66]. Systematical research into 2D topological phonons and their related material realizations is highly required. In 2022, Yu *et al.* [64] discovered the appearance of 2D twofold degenerate quadratic nodal point phonons and presented a guideline for studying the quadratic nodal point in 2D phononic systems via symmetry analysis. In 2020, Li *et al.* [65] proposed that 2D graphene hosts four types of Dirac phonons and a nodal ring phonon in its phonon spectrum. In 2018, Jin *et al.* [66] predicted the appearance of Dirac phonons in 2D hexagonal lattices using first-principles calculations. Note that the linearly dispersed twofold phonon band crossing points in 2D graphene and 2D hexagonal lattices are misclassified as Dirac points because of their historical use in early graphene research [67,68]. The correct name for these twofold degenerate nodal points should be "Weyl" because 2D phononic systems are essentially spinless and because each twofold degenerate band crossing point at $K$ or $K_0$ in 2D graphene and 2D hexagonal lattices is characterized by a 2D Weyl Hamiltonian with a defined chirality.

The study of Dirac phonons in 2D materials is still rather primitive and needs to be undertaken by researchers. In this paper, using 2D spinless phononic systems as targets, we searched through all 80 layer groups (LGs) with time-reversal symmetry $\mathcal{T}$ and identified 7 LG candidates that host Dirac points based on theoretical analysis (see Table I). Moreover, the Dirac points in the phonon dispersions of 2D materials can be divided into essential and accidental degenerate points,

*These authors contributed equally to this work.
†Corresponding author: zzy@mail.buct.edu.cn
‡Corresponding author: xiaotianwang@swu.edu.cn, xiaotianw@uow.edu.au

 

TABLE I. LG candidates [and their corresponding space groups (SGs)] that can host Dirac points at HSPs or on HSLs in 2D phononic systems. This table also includes the locations of the Dirac phonons, the correspondence generators and labels associated with the Dirac points, and the 2D material candidates.

| Dirac phonons at HSPs<br>LG No. | LG symbol | SG No. | SG symbol | Generator | Location | Label | Materials |
|---|---|---|---|---|---|---|---|
| 33 | $pb2_1a$ | 29 | $Pca2_1$ | $C_{2y},\sigma_z,\mathcal{T}$ | $S$ | $T_1T_1$ | $Ni_8As_4Si_4$ |
| 43 | $pbaa$ | 54 | $Pcca$ | $C_{2x},C_{2z},I,\mathcal{T}$ | $S$ | $U_1U_2$ | $C_8H_8$ |
| 45 | $pbma$ | 57 | $Pbcm$ | $C_{2x},C_{2y},I,\mathcal{T}$ | $S$ | $S_1S_2$ | $Pb_4O_4$ |
| Dirac phonons on HSLs<br>LG No. | LG symbol | SG No. | SG symbol | Generator | Location | Label | Materials |
| 29 | $pb2_1m$ | 26 | $Pmc2_1$ | $\sigma_z,C_{2y}\mathcal{T}$ | $Y$-$S$ path | $\{B_1B_1, B_2B_2\}$ | $Mo_2Br_4O_4$ |
| 33 | $pb2_1a$ | 29 | $Pca2_1$ | $\sigma_z,C_{2y}\mathcal{T}$ | $Y$-$S$ path | $\{B_1B_1, B_2B_2\}$ | $Ni_8As_4Si_4$ |
| 40 | $pmam$ | 51 | $Pmma$ | $C_{2y},\sigma_z,C_{2z}\mathcal{T}$ | $X$-$S$ path | $\{A_1A_2, A_3A_4\}$ | |
| 43 | $pbaa$ | 54 | $Pcca$ | $C_{2x},\sigma_z,C_{2z}\mathcal{T}$ | $Y$-$S$ path | $\{A_1A_2, A_3A_4\}$ | $C_8H_8$ |
| 44 | $pbam$ | 55 | $Pbam$ | $C_{2x},\sigma_y,C_{2y}\mathcal{T}$ | $X$-$S$ path<br>$Y$-$S$ path | $\{D_1D_2, D_3D_4\}$ | $Nb_4Te_8Si_2$ |
| 45 | $pbma$ | 57 | $Pbcm$ | $C_{2x},\sigma_y,C_{2y}\mathcal{T}$ | $Y$-$S$ path | $\{C_1C_2, C_3C_4\}$ | $Pb_4O_4$ |
| 63 | $p4/mbm$ | 127 | $P4/mbm$ | $C_{2x},\sigma_y,C_{2y}\mathcal{T}$ | $X$-$M$ path | $\{Y_1Y_2, Y_3Y_4\}$ | $Mg_2N_4$ |

which appear at high-symmetry points (HSPs) and on high-symmetry lines (HSLs), respectively. It is well known that material realization is a prerequisite for studying topological states. Hence, we propose a series of 2D material candidates with six LGs based on first-principles calculations. Our work offers a method for identifying Dirac points in 2D phononic systems and proposes a series of 2D candidate materials with Dirac phonons at HSPs and on HSLs.

## II. SYMMETRY ANALYSIS

In general, the Dirac points in LGs are caused by the four-dimensional (4D) corepresentation of little groups in the Brillouin zone (BZ). Recently, Zhang *et al.* [69] proposed the entire corepresentation of 528 magnetic LGs by restricting specific corepresentations in 3D magnetic space groups. Herein, we present some necessary conditions for the Dirac points in LGs. First, the order of the little cogroup of LGs must be greater than or equal to 4 for Dirac points at HSPs. This can be understood by using the property of characters of projective representations as follows,

$$\sum_i \chi_i^2(e) = |\mathcal{L}|, \tag{1}$$

where $\chi_i(e)$ is the character of an identity element and is equal to the dimension of irreducible representation, and $\mathcal{L}$ is the little cogroup. Notably, the dimension of irreducible representations can be greater than or equal to 2 only for $|\mathcal{L}| \geqslant 4$. Second, antiunitary elements are necessary for the magnetic little cogroup of HSPs. Antiunitary operators play an important role in sticking two 2D irreducible representations together because there is no 4D irreducible representation in LGs. The Dirac point on HSLs is formed by two accidentally intersecting bands. Therefore, each band must be doubly degenerate and belong to different corepresentations. The above symmetry analysis is consistent with Table I.

## III. MATERIAL CANDIDATES WITH DIRAC PHONONS AT HSPS

Table I shows that LGs 33, 43, and 45 should exhibit Dirac points, known as fourfold essential degenerate points, at the $S$ HSP. We supported our symmetry analysis by predicting a series of 2D materials with LGs 33, 43, and 45 and multiple Dirac phonons at the $S$ HSP based on first-principles calculations. The structural models for 2D $Ni_8As_4Si_4$, 2D $C_8H_8$, and 2D $Pb_4O_4$ materials are shown in Figs. 1(a)–1(c), respectively. Note that the structural models for 2D $Ni_8As_4Si_4$ and 2D $Pb_4O_4$ were screened from the Computational 2D Materials Database [70] and 2D Materials Encyclopedia [71], respectively. He *et al.* [72] proposed the structural model for 2D $C_8H_8$ in 2012.

The phonon dispersions of the 2D $Ni_8As_4Si_4$, 2D $C_8H_8$, and 2D $Pb_4O_4$ materials along the $\Gamma$-$X$-$S$-$Y$-$\Gamma$-$S$ high-symmetry paths [see Fig. 1(d)] are shown in Fig. 2 and Figs. S1–S4 [see the Supplemental Material (SM) [73]], respectively. More details about the computational methods can be found in the SM [73]. Notably, multiple Dirac points are observed at the $S$ HSP in the phonon dispersions of the 2D $Ni_8As_4Si_4$, 2D $C_8H_8$, and 2D $Pb_4O_4$ materials, which agree well with the above symmetry analysis. Figure 2(a) shows that there are 12 visible phonon band crossing points with fourfold degeneracies (marked as red dots) at the $S$ HSP. Figure 2(b) shows the enlarged figures of these Dirac phonons (Nos. 1–12), and Fig. S5 shows the 3D plots of these 12 Dirac phonons (Nos. 1–12) (see SM [73]).

Actually, all phonon bands along the $Y$-$S$ and $X$-$S$ high-symmetry paths in 2D materials with LGs 33, 43, and 45 are twofold degenerate. That is, symmetry-enforced twofold degenerate Weyl lines (WLs) should appear along the $Y$-$S$ and $X$-$S$ high-symmetry paths in LGs 33, 43, and 45 (see Table S1). Figure 3(a) shows the enlarged phonon bands around the Dirac point (No. 1) at about 11.22 THz as a typical example. The two WLs that form the Dirac point at the $S$ HSP are highlighted by two colors. We selected some

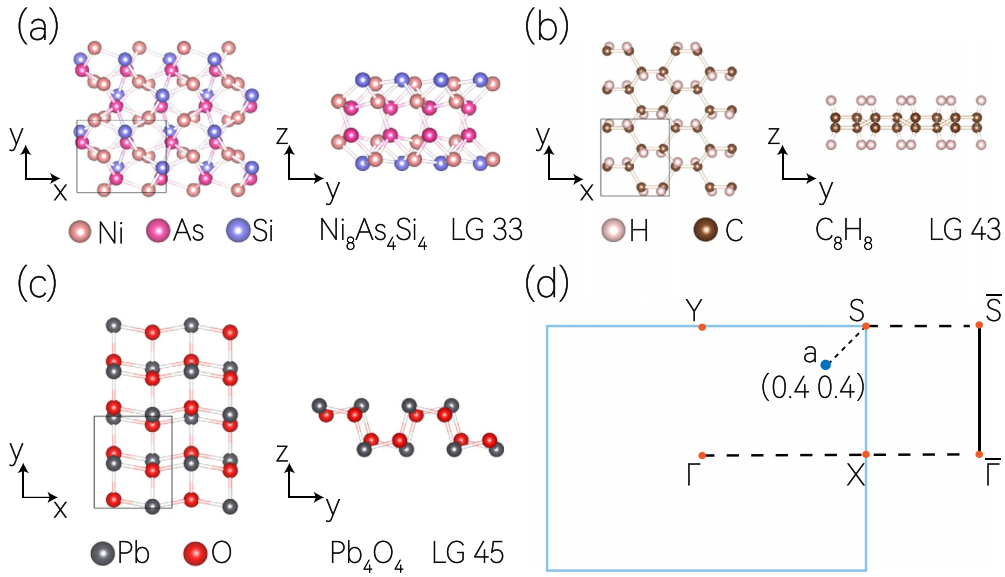


FIG. 1. (a)–(c) Different side views of the structural models for 2D $Ni_8As_4Si_4$, 2D $C_8H_8$, and 2D $Pb_4O_4$. (d) The 2D BZ and its projection to the [100] edge.

symmetry paths, such as $b$-$n$-$b_1$, $c$-$m$-$c_1$, $d$-$p$-$d_1$, and $e$-$o$-$e_1$ [see Fig. 3(b)], and calculated the phonon dispersion along them to confirm that all the phononic crossing points of the two WLs have twofold degeneracies. The $m$ and $n$ were on the $X$-$S$ high-symmetry paths, while $o$ and $p$ were on the $Y$-$S$ paths. Figures 3(c) and 3(d) show that the twofold degenerate Weyl points appeared at the $o$, $p$, $m$, and $n$ symmetry points.

In contrast to 3D systems that have a twofold screw rotation and time-reversal symmetry $\mathcal{T}$ that must lead to a nodal surface at the $k_\perp = \pi$ plane, where it is perpendicular to the screw rotation axis ($S_{2i}$), 2D systems have symmetries (i.e., $S_{2x}\mathcal{T}$ and $S_{2y}\mathcal{T}$) that lack a degree of freedom, resulting in different degeneracies. That is, the WL only inherits the degeneracy on one line of the nodal surface because the BZ is 2D.

The twofold degenerate WLs along the $Y$-$S$ and $X$-$S$ high-symmetry paths intersected at the $S$ HSP and formed a fourfold degenerate point at the $S$ point in LGs 33, 43, and 45. The phonon dispersions around the Dirac points (No. 2 and No. 12) at the $S$ point along the $a$-$S$-$a$ paths are shown in Figs. 4(a) and 4(b), respectively, to verify this. The figures show that the Dirac points have fourfold degeneracies.

Furthermore, we studied the edge states of the Dirac phonons (with No. 2 and No. 12) along [100] [see Fig. 1(d)]. The results are shown in Figs. 4(c) and 4(d), respectively. The positions of the Dirac points (No. 2 and No. 12) are marked by black balls. The edge states noticeably stem from the projection of the Dirac points. Such clean edge states will benefit from follow-up experimental detections using

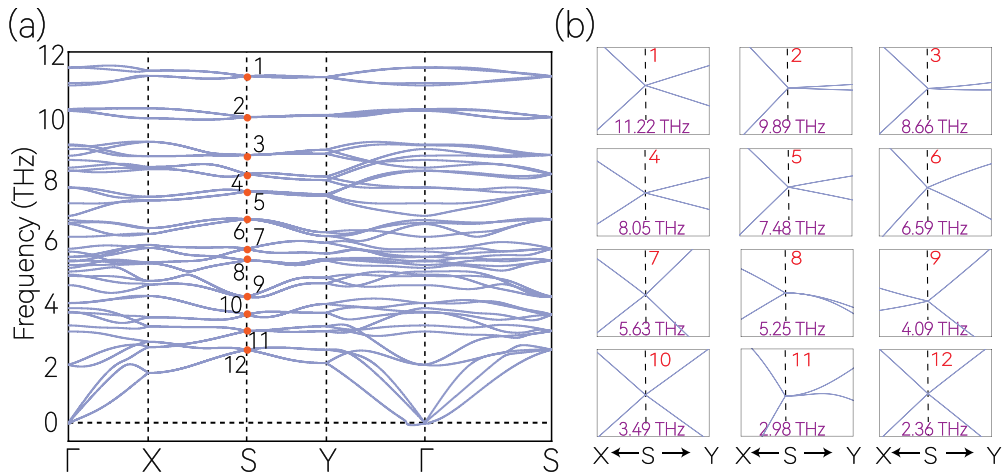


FIG. 2. (a) Phonon dispersions of the 2D $Ni_8As_4Si_4$ primitive cell along the Γ-$X$-$S$-$Y$-Γ-$S$ paths. A supercell of $3 \times 3 \times 1$ is adopted for the calculation of force constants. The Dirac points (labeled with Nos. 1–12) located at different frequencies are marked by red dots. (b) Enlarged phonon bands around the 12 Dirac phonons.

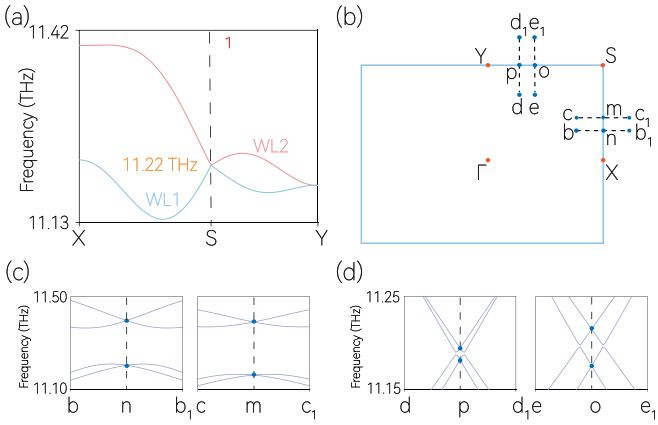


FIG. 3. (a) Enlarged phonon band of the No. 1 Dirac phonon. Two WLs (red and blue colors) appear along the $X$-$S$-$Y$ paths. (b) The 2D BZ and the $b$-$n$-$b_1$, $c$-$m$-$c_1$, $d$-$p$-$d_1$, and $e$-$o$-$e_1$ symmetry paths. (c) and (d) Calculated phonon dispersions along the above-mentioned symmetry paths. The Weyl points in (b)–(d) are indicated by blue dots.

surface-sensitive probes, such as electron energy loss spectroscopy and helium scattering.

## IV. MATERIAL CANDIDATES WITH DIRAC PHONONS ON HSLS

Table I shows that LGs 29, 33, 40, 43, 44, 45, and 63 may host Dirac points on HSLs. Note that the Dirac point along HSLs has an accidental fourfold degeneracy. To support our symmetry analysis, six 2D material candidates with LGs 29, 33, 43, 44, 45, and 63, including $Mo_2Br_4O_4$, $Ni_8As_4Si_4$, $C_8H_8$, $Nb_4Te_8Si_2$, $Pb_4O_4$, and $Mg_2N_4$, are presented in this paper. Figures S6– S18 display the structural models, 2D BZ,

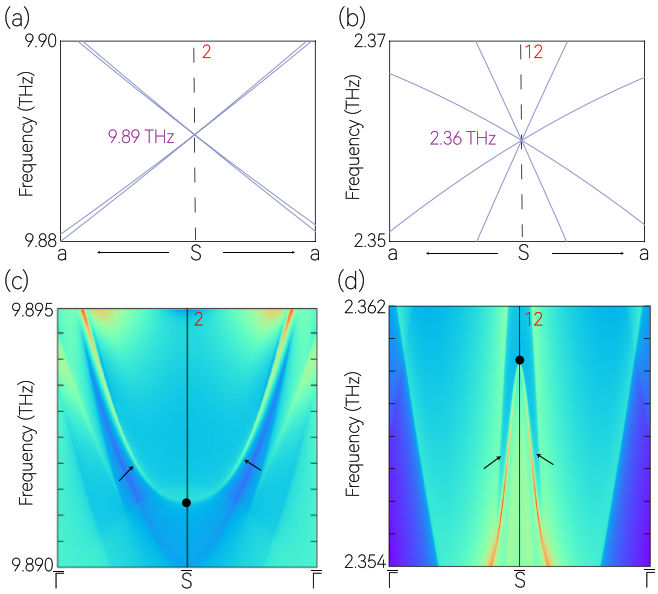


FIG. 4. (a) and (b) Enlarged phonon dispersions around the No. 2 and No. 12 Dirac phonons, respectively. (c) and (d) Edge states of the No. 2 and No. 12 Dirac phonons, respectively. The black arrows in (c) and (d) show the edge states originating from the projections of the No. 2 and No. 12 Dirac points.

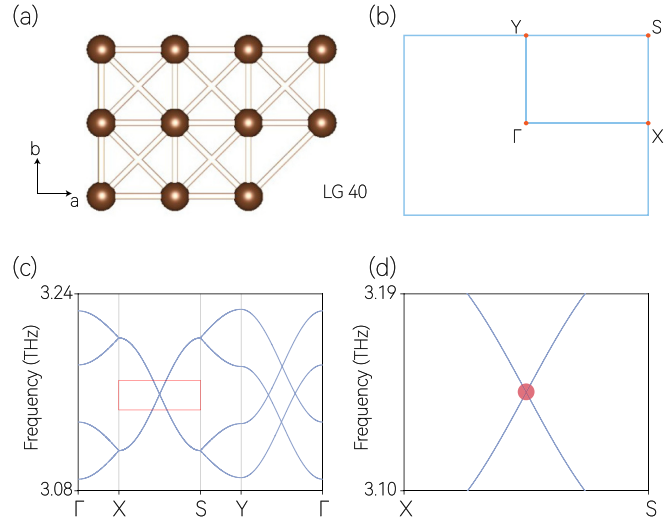


FIG. 5. (a) Spinless TB model with LG 40. (b) The 2D BZ and selected high-symmetry paths. (c) Calculated phonon dispersion for the spinless lattice model with LG 40. The Dirac point location on the $X$-$S$ path is highlighted by a red box. (d) Enlarged phonon dispersion around the Dirac point (marked by a red dot).

and calculated phonon dispersions for these six materials (see SM [73]).

The 2D $Mo_2Br_4O_4$, 2D $Ni_8As_4Si_4$, 2D $C_8H_8$, and 2D $Pb_4O_4$ materials with LGs 29, 33, 43, and 45, respectively, host Dirac points on the $Y$-$S$ path [see Figs. S6(d), S8(d), S10(d), and S15(d) in the SM [73]]. For example, the bands along the $Y$-$S$ path in 2D $C_8H_8$, which has LG 43, are twofold degenerate (see Table S1 in the SM [73]), and two WLs cross each other to form a fourfold degenerate Dirac point around 24 THz [see Figs. S10(d) and S10(e) in the SM [73]]. Furthermore, the 2D $Nb_4Te_8Si_2$ material with LG 44 can host Dirac points on both the $X$-$S$ and $Y$-$S$ paths [see Figs. S12(d)–S12(f) in the SM [73]]. The 2D $Mg_2N_4$ material with LG 63 can host Dirac points on the $X$-$M$ path [see Figs. S17(d) and S17(e) in the SM [73]].

To better view that the crossing points on HSLs are fourfold degenerate Dirac points, we also selected some symmetry paths and calculated the phonon dispersions along the selected $k$ paths for $Mo_2Br_4O_4$, $Ni_8As_4Si_4$, $C_8H_8$, $Nb_4Te_8Si_2$, $Pb_4O_4$, and $Mg_2N_4$. The results are shown in Figs. S7, S9, S11, S13 and S14, S16, and S18, respectively, in the SM [73]. From these figures in the SM [73], one can find the P1 and P3–P8 points on HSLs are fourfold degenerate Dirac points on HSLs.

## V. SPINLESS LATTICE MODELS WITH LG 40

Unfortunately, 2D materials with LG 40 were not discovered in this study. We constructed a tight-binding (TB) model to demonstrate that Dirac points exist on the $X$-$S$ path in 2D with LG 40 in order to aid further investigations. We chose a representation of $u = (u_{A_x}, u_{A_y}, u_{B_x}, u_{B_y})^T$, where $A = (0, 0)$ and $B = (\frac{1}{2}, 0)$, which correspond to the displacements of the $2a$ Wyckoff position along the $x$ and $z$ directions. Thereafter,

the four-band dynamic matrix is satisfied [see Fig. 5(a)],

$$\begin{pmatrix} D_{11} & 0 & D_{13} & 0 \\ & D_{22} & 0 & D_{24} \\ & & D_{11} & 0 \\ \dagger & & & D_{22} \end{pmatrix}, \tag{2}$$

where $D_{11} = e_1 + 2t_1 \cos k_y$, $D_{13} = 2\cos\frac{k_x}{2} t_3$, $D_{22} = e_2 + 2t_2 \cos k_y$, and $D_{24} = 2\cos\frac{k_x}{2} t_4$. The phonon frequency ($\omega$) can be solved using $D(k)u_k = \omega^2 u_k$. Figure 5(b) depicts the phonon dispersion of the spinless lattice model [Eq. (2)] along the $\Gamma$-$X$-$S$-$Y$-$\Gamma$ paths. We set $t_1 = -0.146$, $t_2 = 0.146$, $t_3 = -0.074$, and $t_4 = -0.07$ for the bands in Fig. 5(b). Figures 5(c) and 5(d) show that a fourfold degenerate Dirac point appeared on the $X$-$S$ path and was formed by the crossing of two WLs. This simple spinless model may serve as a starting point for future research into the Dirac points in LG 40.

## VI. SUMMARY

In conclusion, we studied the symmetry conditions of 80 LGs and discovered that Dirac phonons can appear in 7 of the 80 LGs. Specifically, Dirac phonons at the $S$ HSP can only appear in LGs 33, 43, and 45, whereas Dirac phonons on HSLs can appear in LGs 29, 33, 40, 43, 44, 45, and 63. Thereafter, we predicted several 2D materials that host fourfold degenerate Dirac phonons at HSPs and on HSLs. Note that Chen *et al.* [51] reported the existence of fourfold degenerate Dirac points on HSLs or at HSPs in 3D phononic systems in 2021. However, an exploration of the fourfold degenerate Dirac points in 2D phononic systems has been lacking. Hence, this work provides a guideline for studying the fourfold degenerate Dirac points in 2D phononic systems. More importantly, this work contributes to the material realization of fourfold degenerate Dirac points in 2D phononic systems. Our work can be viewed as a guide for investigating not only fourfold degenerate Dirac points in 2D phononic systems but also other types of emergent particles in 2D phononic systems.

## ACKNOWLEDGMENT

This work was supported by the National Key R&D Program of China (No. 22022YFA1402600), the National Natural Science Foundation of China (Grant No. 12004028), and the Natural Science Foundation of Chongqing (No. CSTB2022NSCQ-MSX0283).

[1] A. Stern and N. H. Lindner, Science **339**, 1179 (2013).
[2] F. D. M. Haldane, Rev. Mod. Phys. **89**, 040502 (2017).
[3] N. Hao and J. Hu, Natl. Sci. Rev. **6**, 213 (2019).
[4] Z.-M. Yu, Z. Zhang, G.-B. Liu, W. Wu, X.-P. Li, R.-W. Zhang, S. A. Yang, and Y. Yao, Sci. Bull. **67**, 375 (2022).
[5] W. Wu, Y. Liu, S. Li, C. Zhong, Z.-M. Yu, X.-L. Sheng, Y. X. Zhao, and S. A. Yang, Phys. Rev. B **97**, 115125 (2018).
[6] K. Wang, J.-X. Dai, L. B. Shao, S. A. Yang, and Y. X. Zhao, Phys. Rev. Lett. **125**, 126403 (2020).
[7] L. Cao, G. Zhou, Q. Wu, S. A. Yang, H. Y. Yang, Y. S. Ang, and L. K. Ang, Phys. Rev. Appl. **13**, 054030 (2020).
[8] C. Chen, X.-T. Zeng, Z. Chen, Y. X. Zhao, X.-L. Sheng, and S. A. Yang, Phys. Rev. Lett. **128**, 026405 (2022).
[9] Q. Wan, T. Y. Yang, S. Li, M. Yang, Z. Zhu, C. L. Wu, C. Peng, S. K. Mo, W. Wu, Z. H. Chen, Y. B. Huang, L. L. Lev, V. N. Strocov, J. Hu, Z. Q. Mao, H. Zheng, J. F. Jia, Y. G. Shi, S. A. Yang, and N. Xu, Phys. Rev. B **103**, 165107 (2021).
[10] Z. Zhu, Y. Liu, Z.-M. Yu, S.-S. Wang, Y. X. Zhao, Y. Feng, X.-L. Sheng, and S. A. Yang, Phys. Rev. B **98**, 125104 (2018).
[11] S. A. Yang, H. Pan, and F. Zhang, Phys. Rev. Lett. **113**, 046401 (2014).
[12] S. Li, Y. Liu, B. Fu, Z.-M. Yu, S. A. Yang, and Y. Yao, Phys. Rev. B **97**, 245148 (2018).
[13] J.-Y. You, C. Chen, Z. Zhang, X.-L. Sheng, S. A. Yang, and G. Su, Phys. Rev. B **100**, 064408 (2019).
[14] X. Zhang, Z.-M. Yu, Z. Zhu, W. Wu, S.-S. Wang, X.-L. Sheng, and S. A. Yang, Phys. Rev. B **97**, 235150 (2018).
[15] Z. Zhu, Z.-M. Yu, W. Wu, L. Zhang, W. Zhang, F. Zhang, and S. A. Yang, Phys. Rev. B **100**, 161401(R) (2019).
[16] A. A. Burkov, Nat. Mater. **15**, 1145 (2016).
[17] B. Q. Lv, T. Qian, and H. Ding, Rev. Mod. Phys. **93**, 025002 (2021).
[18] C. Fang, L. Lu, J. Liu, and L. Fu, Nat. Phys. **12**, 936 (2016).
[19] C. Fang, M. J. Gilbert, X. Dai, and B. A. Bernevig, Phys. Rev. Lett. **108**, 266802 (2012).
[20] J. Chen, H. Li, B. Ding, H. Zhang, E. Liu, and W. Wang, Appl. Phys. Lett. **118**, 031901 (2021).
[21] X. C. Sun, C. He, X. P. Liu, M. H. Lu, S. N. Zhu, and Y. F. Chen, Prog. Quantum Electron. **55**, 52 (2017).
[22] A. B. Khanikaev and G. Shvets, Nat. Photonics **11**, 763 (2017).
[23] T. Ozawa, H. M. Price, A. Amo, N. Goldman, M. Hafezi, L. Lu, M. C. Rechtsman, D. Schuster, J. Simon, O. Zilberberg, and I. Carusotto, Rev. Mod. Phys. **91**, 015006 (2019).
[24] L. Lu, J. D. Joannopoulos, and M. Soljacic, Nat. Photonics **8**, 821 (2014).
[25] G. Arregui, O. Ortíz, M. Esmann, C. M. Sotomayor-Torres, C. Gomez-Carbonell, O. Mauguin, B. Perrin, A. Lemaître, P. D. García, and N. D. Lanzillotti-Kimura, APL Photonics **4**, 030805 (2019).
[26] S. Park, Y. Hwang, H. C. Choi, and B. J. Yang, Nat. Commun. **12**, 6781 (2021).
[27] Z.-K. Ding, Y.-J. Zeng, H. Pan, N. Luo, J. Zeng, L.-M. Tang, and K.-Q. Chen, Phys. Rev. B **106**, L121401 (2022).
[28] Z. Yang, F. Gao, X. Shi, X. Lin, Z. Gao, Y. Chong, and B. Zhang, Phys. Rev. Lett. **114**, 114301 (2015).
[29] P. Zhou, G. G. Liu, Y. Yang, Y.-H. Hu, S. Ma, H. Xue, Q. Wang, L. Deng, and B. Zhang, Phys. Rev. Lett. **125**, 263603 (2020).
[30] G.-G. Liu, Y. Yang, X. Ren, H. Xue, X. Lin, Y.-H. Hu, H.-X. Sun, B. Peng, P. Zhou, Y. Chong, and B. Zhang, Phys. Rev. Lett. **125**, 133603 (2020).
[31] Y. Liu, X. Chen, and Y. Xu, Adv. Funct. Mater. **30**, 1904784 (2020).
[32] Y. Liu, Y. Xu, and W. Duan, Research **2019**, 5173580 (2019).
[33] Y. Liu, Y. Xu, and W. Duan, Natl. Sci. Rev. **5**, 314 (2018).

[34] Y. Liu, N. Zou, S. Zhao, X. Chen, Y. Xu, and W. Duan, Nano Lett. **22**, 2120 (2022).

[35] X.-Q. Chen, J. Liu, and J. Li, Innovation **2**, 100134 (2021).

[36] J. Chen, J. He, D. Pan, X. Wang, N. Yang, J. Zhu, S. A. Yang, and G. Zhang, Sci. China: Phys., Mech. Astron. **65**, 117002 (2022).

[37] J. Chen, X. Xu, J. Zhou, and B. Li, Rev. Mod. Phys. **94**, 025002 (2022).

[38] N. Li, J. Ren, L. Wang, G. Zhang, P. Hänggi, and B. Li, Rev. Mod. Phys. **84**, 1045 (2012).

[39] J. Li, J. Liu, S. A. Baronett, M. Liu, L. Wang, R. Li, Y. Chen, D. Li, Q. Zhu, and X. Chen, Nat. Commun. **12**, 1204 (2020).

[40] T. Zhang, Z. Song, A. Alexandradinata, H. Weng, C. Fang, L. Lu, and Z. Fang, Phys. Rev. Lett. **120**, 016401 (2018).

[41] H. Miao, T. T. Zhang, L. Wang, D. Meyers, A. H. Said, Y. L. Wang, Y. G. Shi, H. M. Weng, Z. Fang, and M. P. M. Dean, Phys. Rev. Lett. **121**, 035302 (2018).

[42] X. Wang, T. Yang, Z. Cheng, G. Surucu, J. Wang, F. Zhou, Z. Zhang, and G. Zhang, Appl. Phys. Rev. **9**, 041304 (2022).

[43] J. Wang, H. Yuan, Y. Liu, G. Zhang, and X. Wang, Appl. Phys. Lett. **121**, 192201 (2022).

[44] Q.-B. Liu, Z. Wang, and H.-H. Fu, Phys. Rev. B **103**, L161303 (2021).

[45] Q.-B. Liu, Y. Qian, H.-H. Fu, and Z. Wang, npj Comput. Mater. **6**, 95 (2020).

[46] R. Wang, B. W. Xia, Z. J. Chen, B. B. Zheng, Y. J. Zhao, and H. Xu, Phys. Rev. Lett. **124**, 105303 (2020).

[47] Y. J. Jin, Z. J. Chen, X. L. Xiao, and H. Xu, Phys. Rev. B **103**, 104101 (2021).

[48] G. Ding, F. Zhou, Z. Zhang, Z.-M. Yu, and X. Wang, Phys. Rev. B **105**, 134303 (2022).

[49] M. Zhong, Y. Han, J. Wang, Y. Liu, X. Wang, and G. Zhang, Phys. Rev. Mater. **6**, 084201 (2022).

[50] Z. Huang, Z. Chen, B. Zheng, and H. Xu, npj Comput. Mater. **6**, 87 (2020).

[51] Z. J. Chen, R. Wang, B. W. Xia, B. B. Zheng, Y. J. Jin, Y.-J. Zhao, and H. Xu, Phys. Rev. Lett. **126**, 185301 (2021).

[52] Y. Feng, C. Xie, H. Chen, Y. Liu, and X. Wang, Phys. Rev. B **106**, 134307 (2022).

[53] S. Singh, Q. S. Wu, C. Yue, A. H. Romero, and A. A. Soluyanov, Phys. Rev. Mater. **2**, 114204 (2018).

[54] P. C. Sreeparvathy, C. Mondal, C. K. Barman, and A. Alam, Phys. Rev. B **106**, 085102 (2022).

[55] J.-Y. You, X.-L. Sheng, and G. Su, Phys. Rev. B **103**, 165143 (2021).

[56] Y. J. Jin, Z. J. Chen, B. W. Xia, Y. J. Zhao, R. Wang, and H. Xu, Phys. Rev. B **98**, 220103(R) (2018).

[57] C. Xie, Y. Liu, Z. Zhang, F. Zhou, T. Yang, M. Kuang, X. Wang, and G. Zhang, Phys. Rev. B **104**, 045148 (2021).

[58] F. Zhou, Z. Zhang, H. Chen, M. Kuang, T. Yang, and X. Wang, Phys. Rev. B **104**, 174108 (2021).

[59] F. Zhou, H. Chen, Z.-M. Yu, Z. Zhang, and X. Wang, Phys. Rev. B **104**, 214310 (2021).

[60] G. Liu, Y. Jin, Z. Chen, and H. Xu, Phys. Rev. B **104**, 024304 (2021).

[61] C. Xie, H. Yuan, Y. Liu, X. Wang, and G. Zhang, Phys. Rev. B **104**, 134303 (2021).

[62] B. Peng, S. Murakami, B. Monserrat, and T. Zhang, npj Comput. Mater. **7**, 195 (2021).

[63] W.-W. Yu, Y. Liu, L. Tian, T. He, X. Zhang, and G. Liu, J. Phys.: Condens. Matter **34**, 155703 (2022).

[64] W.-W. Yu, Y. Liu, W. Meng, H. Liu, J. Gao, X. Zhang, and G. Liu, Phys. Rev. B **105**, 035429 (2022).

[65] J. Li, L. Wang, J. Liu, R. Li, Z. Zhang, and X.-Q. Chen, Phys. Rev. B **101**, 081403(R) (2020).

[66] Y. Jin, R. Wang, and H. Xu, Nano Lett. **18**, 7755 (2018).

[67] S. A. Yang, SPIN **06**, 1640003 (2016).

[68] X. Feng, J. Zhu, W. Wu, and S. A. Yang, Chin. Phys. B **30**, 107304 (2021).

[69] Z. Zhang, W. Wu, G.-B. Liu, Z.-M. Yu, S. A. Yang, and Y. Yao, arXiv:2210.11080.

[70] https://cmrdb.fysik.dtu.dk/c2db/row/As4Si4Ni8-0c60c11fbd24.

[71] http://www.2dmatpedia.org/2dmaterials/doc/2dm-3669.

[72] C. He, C. X. Zhang, L. Z. Sun, N. Jiao, K. W. Zhang, and J. Zhong, Phys. Status Solidi RRL **6**, 427 (2012).

[73] See Supplemental Material at http://link.aps.org/supplemental/10.1103/PhysRevB.106.214317 for the computational methods, the candidate LGs that can host WL along HSLs in 2D phononic systems, and the structural models, 2D BZ, 3D plots of Dirac points, and the calculated phonon dispersions for $Mo_2Br_4O_4$, $Ni_8As_4Si_4$, $C_8H_8$, $Nb_4Te_8Si_2$, $Pb_4O_4$, and $Mg_2N_4$ with LGs 29, 33, 43, 44, 45, 63, which includes Refs. [70–72,74–81].

[74] J. Hafner, J. Comput. Chem. **29**, 2044 (2008).

[75] P. E. Blöchl, Phys. Rev. B **50**, 17953 (1994).

[76] J. P. Perdew, K. Burke, and M. Ernzerhof, Phys. Rev. Lett. **77**, 3865 (1996).

[77] A. Togo and I. Tanaka, Scr. Mater. **108**, 1 (2015).

[78] Q. Wu, S. Zhang, H.-F. Song, M. Troyer, and A. A. Soluyanov, Comput. Phys. Commun. **224**, 405 (2018).

[79] Z. Zhang, Z.-M. Yu, G. B. Liu, and Y. Yao, arXiv:2201.11350.

[80] https://cmrdb.fysik.dtu.dk/c2db/row/Mo2Br4O4-7a7b281fd1f2.

[81] https://cmrdb.fysik.dtu.dk/c2db/row/Si2Nb4Te8-1d32f2bca255.